

ARTICLES

Energy dependence of analyzing power A_y and cross section for $p + d$ scattering below 18 MeV

K. Sagara, H. Oguri,* S. Shimizu,† K. Maeda, H. Nakamura, T. Nakashima, and S. Morinobu
Department of Physics, Kyushu University, Hakozaki, Fukuoka 812, Japan

(Received 29 September 1993)

The vector analyzing power $A_y(\theta)$ of the ${}^2\text{H}(\vec{p}, p){}^2\text{H}$ scattering has been measured at $E_p = 5, 6, 6.5, 7, 8, 8.5, 9, 10, 12, 14, 16,$ and 18 MeV with a typical statistical accuracy of 0.0009 and an uncertainty in the beam polarization of less than 0.7% . The differential cross section $\sigma(\theta)$ of the ${}^2\text{H}(p, p){}^2\text{H}$ scattering has also been measured with a typical uncertainty of 0.8% using unpolarized beams of the same energies and of $2, 2.5, 3,$ and 4 MeV. A large discrepancy of about 25% between the experiment and the Faddeev calculation with the Paris NN potential is observed at the maximum of $A_y(\theta)$ around $\theta_{c.m.} = 120^\circ$. This discrepancy is shown to be reduced by modifying LS force in the NN potential, though a discrepancy still remains in the energy dependence of the $A_y(\theta)$ maximum. At the minimum of $\sigma(\theta)$ around $\theta_{c.m.} = 120^\circ$, a large discrepancy ranging from -19% at 2 MeV to $+24\%$ at 18 MeV is observed between the experiment and the calculations with either of the original and the LS -modified NN potentials. This indicates that an improvement is also necessary in the scalar part of the potential. The difference in the $A_y(\theta)$ maximum between the $\vec{p} + d$ and the $\vec{n} + d$ scatterings is discussed.

PACS number(s): 25.10.+s, 24.70.+s, 25.45.De

I. INTRODUCTION

Recently, three-body Faddeev calculations for the $n + d$ scattering have been performed [1,2] using realistic nucleon-nucleon (NN) potentials in their original forms. This progress has enabled an examination of various types of realistic NN potentials by contrast of the predictions with the experimental data on the $N + d$ scattering states. Precise measurements of the vector analyzing power A_y of the $\vec{n} + d$ scattering have also been made recently at incident neutron energies of 3 – 14 MeV [3–7] with accuracies (3 – 6%) comparable to those of the existing A_y data for the $\vec{p} + d$ scattering below 20 MeV [8–12].

Comparisons of the Faddeev calculations with these data have revealed the presence of a large deviation (about 25%) of the calculation from the experiment around the maximum of the angular distribution of A_y (hereafter referred as A_y peak) below 20 MeV. Witala and Glöckle [13] have found that this discrepancy can be removed by introducing strong charge independence breaking (CIB) in the 3P_J -state NN interactions, while Takemiya [14] has proposed a modification of the short

range part of the LS force in the NN potential without CIB. Both the results indicate a necessity of improving the P -state NN interactions. To find the true cause for this discrepancy, however, further systematic and detailed comparison of theoretical predictions with more precise experimental data are necessary. For this purpose, high precision data for A_y below 20 MeV are of fundamental importance.

The difference in A_y peak heights between the $\vec{n} + d$ and the $\vec{p} + d$ scatterings is about 10% in the energy range below 14 MeV. If it is not fully attributed to Coulomb force in the $p + d$ system, the difference means a presence of charge symmetry breaking (CSB) in the nuclear interactions. Witala and Glöckle [13] have reproduced the difference by introducing strong CSB in the 3P_J -state NN interactions without including Coulomb force in the calculation. Berthold, Stadler, and Zankel [15] have recently succeeded in treating Coulomb force nearly correctly in the $p + d$ scattering below the deuteron breakup threshold ($E_p = 3.3$ MeV), and found that the Coulomb force effect is significant for A_y even at backward angles around 120° where the A_y peak appears. As the energy increases, it is expected that the Coulomb force effect becomes less important and the CSB effect, if existed, becomes relatively conspicuous. Hence, the development of a correct treatment of Coulomb force above the threshold is highly desired. Also to be mentioned is that the accuracy of the existing A_y data of both the $\vec{p} + d$ and the $\vec{n} + d$ scatterings is still insufficient for the quantitative study of the CSB effect. An accuracy of about 1% is required.

Large discrepancies between the calculation and the

*Present address: Accelerator Engineering Laboratory, Japan Atomic Energy Research Institute, Tokai-mura 319-11, Japan.

†Present address: Department of Mechanical Engineering, Yamaguchi University, Ube 755, Japan.

experiment such as found for A_y have not been reported so far for the cross section and other analyzing powers. However, it is also very important to make precise and systematic measurements on these observables over a wide energy range for comparisons with the Faddeev calculations. Such comparisons would enable improvements of the various parts of the NN interaction.

In order to facilitate stringent examinations of the NN potentials in the $3N$ system, we have initiated systematic measurements of all the vector and tensor analyzing powers and the differential cross section for the $p + d$ scattering below 18 MeV with accuracies down to 1%. In this paper, the first experimental results on A_y and the cross section are presented and are compared with the Faddeev calculation [16] based on the Paris NN potential. The $\bar{p} + d$ A_y data are also compared with the existing $\bar{n} + d$ A_y data to see the CSB effect.

II. EXPERIMENT ON ANALYZING POWER

The angular distribution of A_y of the ${}^2\text{H}(\vec{p}, p){}^2\text{H}$ scattering was measured at $E_p^{\text{lab}} = 5.00, 6.00, 6.50, 7.00, 8.00, 8.50, 9.00, 10.00, 12.00, 14.00, 16.00,$ and 18.00 MeV. These energies were chosen to see the systematic behavior of A_y and to enable a direct comparison with the existing ${}^2\text{H}(\vec{n}, n){}^2\text{H}$ data at 5.0, 6.5, 8.5, 10.0, 12.0, and 14.1 MeV.

A. Polarized proton beam

A polarized proton beam was produced in a Lamb-shift type ion source at the Kyushu University tandem accelerator facility. After the polarized beam was accelerated up to 30 keV, the polarization axis was rotated into the vertical direction in a Wien-filter type spin precessor. The beam was accelerated by the tandem accelerator, momentum analyzed by a 90° bending magnet, and focused on a target placed at the center of a scattering chamber of 1 m in diameter. The maximum beam current on the target was $0.3 \mu\text{A}$. The spin direction was flipped upward and downward every 10 s by changing the magnetic field in the spin filter of the ion source.

The beam polarization was measured throughout the experiment by a proton beam polarimeter [17] placed at the downstream end of the scattering chamber. The polarimeter had a ${}^4\text{He}$ gas target and four (left, right, upper, and lower) counters to detect protons elastically scattered at 113° . The left and right counters were used to measure the asymmetry of the $p+{}^4\text{He}$ scattering caused by the beam polarization. The upper and lower counters were used to monitor the beam charges so as to determine the polarizations of the spin-up and spin-down beams separately. The typical polarization was 75% for the spin-up beam and 53% for the spin-down beam. The beam polarization was determined within a statistical accuracy of 0.5% in a typical experimental run of 10 min measurement.

The effective analyzing power of the beam polarimeter was calculated based on the three sets of the $p+{}^4\text{He}$

phase shifts [18–20] taking the finite sizes of the counter slits into account. The three calculated results coincided with each other within 0.1% at $E_p = 6.5\text{--}15$ MeV, while the difference among them increased up to 0.7% at 5 and 18 MeV. We adopted the result from the phase shifts of Ref. [20] because it showed an overall consistency with the other results in the whole energy range of present concern. The energy dependence of the effective analyzing power of the beam polarimeter was checked in a separate experiment. The beam polarization was measured using the $p+{}^4\text{He}$ scattering in the scattering chamber, and the analyzing power of the polarimeter was measured simultaneously for the beam energies degraded by metal foils placed in front of the polarimeter. For the same beam polarization, the ratio of the two $p+{}^4\text{He}$ analyzing powers was obtained in the energy range of 5–18 MeV. The results were in good agreement with the adopted calculation. The overall uncertainty in the effective analyzing power of the polarimeter was estimated to be 0.7% for the beam energy of 5 MeV, 0.5% for 6–6.5 MeV, 0.4% for 7–9 MeV, 0.3% for 10–12 MeV, 0.4% for 14 MeV, 0.5% for 16 MeV, and 0.7% for 18 MeV.

B. Experimental setup

A gas cell for the D_2 target, shown in Fig. 1, was placed in vacuum at the center of the scattering chamber. The cell was equipped with two sets of windows for the forward-angle ($\theta_{\text{lab}} \leq 16^\circ$) and backward-angle ($16^\circ \leq \theta_{\text{lab}}$) measurements. The angular spread of particles due to multiple scattering in a window foil is roughly

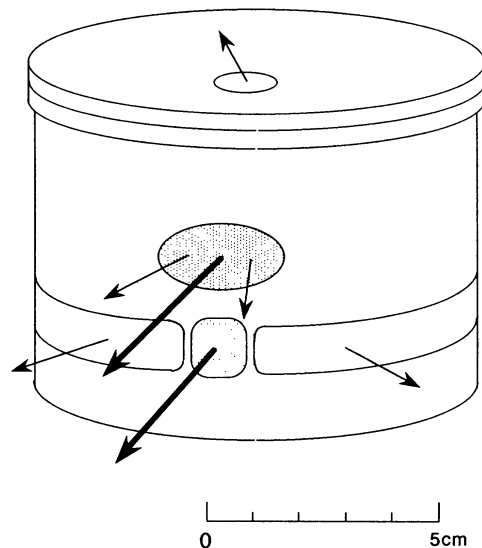


FIG. 1. Perspective view of the target gas cell. The thick and thin arrows indicate the incident beams and scattered particles, respectively. The upper and lower windows on the side were used for the measurements at forward angles ($\theta_{\text{lab}} \leq 16^\circ$) and backward angles, respectively. Through the window at the top, the elastic scattering was measured to monitor the target gas pressure. For the details of the window foils, see text. The shaded areas show the metal foils.

proportional to \sqrt{Zt}/E , where E is the particle energy, Z and t are, respectively, the atomic number and the thickness (surface density) of the foil material. To reduce the spread, thin and low- Z foils were adopted for the target cell windows, i.e., 4- μm -thick aluminum foils for the beam entrance windows, a 2.2- μm -thick Havar foil, and a 4- μm -thick aluminum foil for the upper and the lower beam exit windows, respectively, and 6- μm -thick mylar foils for the side windows (see Fig. 1). The angular spread (FWHM) was estimated [21] to be $\pm 0.41^\circ$ for 5 MeV protons in the beam entrance window, and $\pm 0.51^\circ$ ($\pm 0.54^\circ$) for 2.5 MeV protons (deuterons) in the side windows. The Havar and Mylar foils were found to withstand the inner gas pressure of up to 2 atm. A pressure limit was placed by the aluminum foil at 1.2 atm which was achieved by curving the window frame in a small radius of curvature of 6 mm. The experiment was performed at the target gas pressure of 0.3–0.8 atm.

Two particle counters were placed in the scattering chamber symmetrically to the left and the right of the beam axis in the horizontal plane to detect the scattered protons as well as the recoil deuterons from the $p + d$ scattering. Surface barrier Si detectors of 1 mm in thickness were used for the counters in the measurements at beam energies below 9 MeV. At higher beam energies, counter telescopes each consisting of a 0.1-mm-thick Si detector and a 3-mm-thick Si(Li) detector were used to separate the recoil deuterons from protons coming from the deuteron breakup reaction.

Double slit systems were used to define the effective target thickness viewed by the counters, and the target height was determined by the width of the beam itself. In the forward angle ($\theta_{\text{lab}} \leq 24^\circ$) measurements, each of the double slit systems consisted of a vertical slit of 2 mm width and a 4-mm-wide and 9-mm-high slit aperture placed at 5 cm and 40 cm apart from the target center, respectively. In the backward angle measurement, 1.5 times large slit apertures both in width and height were used. The effective angular spreads (FWHM), defined by the slit systems and the finite extension of the target gas volume, were calculated in the horizontal plane to be $\pm 0.33^\circ$ and $\pm 0.49^\circ$ in the forward and backward measurements, respectively. The direction of the beam axis was determined to $\pm 0.1^\circ$ by measuring the Rutherford scattering at very forward angles on both sides of the beam axis.

C. Measurement and data reduction

Both the scattered protons and recoil deuterons from the ${}^2\text{H}(p,p){}^2\text{H}$ scattering were measured in the angular range of 10° – 52° . The c.m. angular range covered was 14.98° – 75.20° in the proton measurement and 160° – 76° in the deuteron counting in the nonrelativistic limit. To confirm the consistency between the proton data and the deuteron data, measurements were made at several backward angles ($\theta_{\text{lab}} > 52^\circ$). Consistency checks were also made at $\theta_{\text{lab}} = 16^\circ$ for the measurements with the different (the upper and the lower) windows of the target cell (see Fig. 1) and at $\theta_{\text{lab}} = 20^\circ$ – 24° for the different

apertures of the double slit systems.

The beam intensity was controlled so as to keep the counting rate in each detector below 6×10^3 counts/sec which caused a counting loss of about 2.5%. The dead time in the polarimeter was always less than 0.3%. Both the contributions in the corrections of the analyzing power were negligibly small. At most of the angles, more than 2×10^6 events of protons as well as of deuterons were accumulated in both the left and the right counters.

The analyzing powers from the left and the right counters, A_L and A_R , were calculated as

$$A_L = 2x/[(p^+ + p^-) - (p^+ - p^-)x], \quad (1)$$

$$A_R = 2y/[(p^+ + p^-) + (p^+ - p^-)y], \quad (2)$$

where + and – suffices correspond to the spin-up and spin-down beams, respectively, and p denotes the beam polarization. The experimental asymmetries x and y are defined as

$$x = (L^+ - L^-)/(L^+ + L^-), \quad (3)$$

$$y = (R^- - R^+)/(R^+ + R^-), \quad (4)$$

with L and R being the particle counts per unit beam charge in the left and the right counters, respectively.

The proton and deuteron counts were obtained by integrating the energy spectra of the particles around the respective peaks. To see the effect of the background in the spectra, the integration range for a peak was changed systematically from the full width at 1/50 maximum to the full width at half maximum. The resulting asymmetry was found to increase by 0.0002 or less, which was well within the statistical error, except at a few forward angles where Rutherford peaks from the target contaminants (C, N, and O) interfered with the proton peak. The integration range of the width at 1/20 maximum was generally adopted to calculate the final asymmetry, and the range was reduced, if necessary, to eliminate contaminant contribution, down to the width at half maximum.

The derived A_L and A_R agreed with each other within statistical errors and were averaged to give the final analyzing power A_y . The typical statistical error in A_y was 0.0009, including the contribution of less than 0.0006 from the beam polarization measurement. The uncertainty in the scale of A_y came from the uncertainty in the polarimeter analyzing power which was estimated to be 0.3–0.7% as described in Sec. II A.

III. EXPERIMENT ON DIFFERENTIAL CROSS SECTION

The differential cross section of the ${}^2\text{H}(p,p){}^2\text{H}$ scattering was measured using an unpolarized proton beam at 16 points of energy in the range from 2 to 18 MeV including those in the A_y measurement. The experimental setup was basically the same as described in Sec. II B.

A. Experimental setup

For the lowest beam energy of 2 MeV, the scattered protons and deuterons of energies down to 1 MeV were to be measured. To cope with the large multiple scattering effect for such low energy beams and scattered particles, thin foils were used for the target cell windows; 2 μm aluminum foils for the beam entrance windows and 1.5 μm Mylar foils for the side windows (see Fig. 1). The target D_2 gas pressure was 0.2 atm. Since the target gas was observed to leak through the Mylar windows at a rate of about 0.3% per hour, the gas pressure was monitored by counting elastically scattered protons with a counter placed above the target cell.

The incident beam was collimated by a slit of a 2 mm \times 3 mm aperture placed at 12 cm upstream position from the target center, and collected by a Faraday cup of 7 cm in diameter at 50 cm downstream from the target center. It was confirmed in a separate experiment that the full beam charge was collected by the Faraday cup for the beam energies above 4 MeV, while $1.9 \pm 0.2\%$ and $3.8 \pm 0.4\%$ of the beam charge escaped the measurement at 3 and 2 MeV, respectively, due mainly to the multiple scattering effect in the target cell windows. The measured charge was corrected for the effect in the beam energy range below 3 MeV.

To reduce the experimental errors, two counters were placed symmetrically to the left and the right of the beam axis as in the A_y measurement. The counters were equipped with double slits of the same geometry except for the apertures. A pair of a vertical slit of 2 mm in width and a 4-mm-wide and 9-mm-high slit aperture (A system) was used for the measurement at the beam energies of 5–9 MeV, while a pair of the same vertical slit and a 6 mm \times 6 mm aperture (B system) was used at the other beam energies. Consistency of the measurements was confirmed using both the systems at several angles in the energy range 5–9 MeV. The effective angular spread of the A (B) slit system was calculated to be $\pm 0.33^\circ$ ($\pm 0.49^\circ$) in the lab system.

B. Measurement and data reduction

Both the scattered protons and the recoil deuterons from the $p + d$ scattering were again measured using the left and the right counters. The deuterons were separated from the continuum proton spectra due to the deuteron breakup reaction using the counter telescopes. Measurements were made in the lab angular range 16° – 52° at incident beam energies below 10 MeV for protons and below 4 MeV for deuterons, and in the range 10° – 52° at higher energies.

A typical energy spectrum of the protons is shown in Fig. 2. The main peak from the ${}^2\text{H}(p,p)$ scattering and two peaks due to hydrogen and heavy contaminants (C,N,O) are seen together with the continuum spectrum due to the deuteron breakup. The main peak has a long tail at its low energy side. The shape and the relative height of the tail were investigated in the single peak spectra of deuterons detected by the counter telescopes,

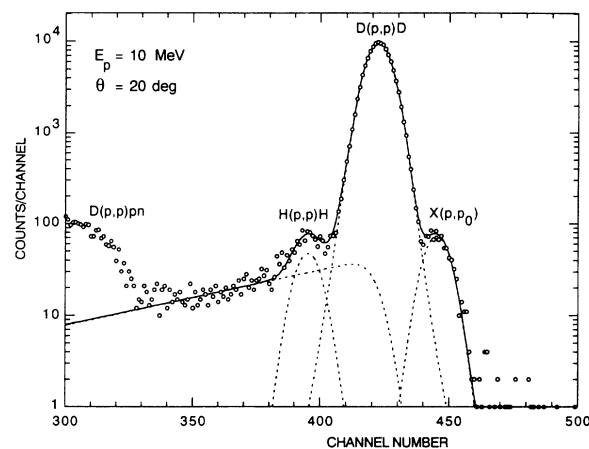


FIG. 2. Typical proton energy spectrum for the ${}^2\text{H}(p,p)$ scattering observed at $\theta_{\text{lab}} = 20^\circ$ for the beam energy of 10 MeV. The peaks from the target contaminants of hydrogen and heavier elements X (C, N, and O) are seen at the shoulders of the main peak. The spectrum was decomposed into Gaussian-like peak functions and exponential tail functions (see text). Recoil deuterons have been separated out in the figure using a counter telescope.

and by measuring proton spectra from the $p + p$ scattering at some scattering angles at several incident energies. It was found that the tail shape was well expressed by an exponential function, and the relative height of the tail was a slowly varying function of the incident beam energy and the laboratory angle. Based on these observations, the shape and the relative height of the tail were estimated for the whole angles and energies as well as for the slit geometries employed.

The particle counts in the main peak was obtained by subtracting the tail and the contaminant contributions from the spectrum in the following procedure. First, the shape of the peak above $1/20$ of the maximum was fitted to a function of the channel E , which resembles the Gaussian function, as expressed as

$$f(E) = Y_0 \left/ \left(1 + \sum_{n=1}^5 C_n (E - E_0)^{2n} \right) \right., \quad (5)$$

where E_0 and Y_0 are, respectively, the position and the height of the peak. The coefficients C_n were determined separately for the low-energy and the high-energy sides of the peak. Next, the exponential tail function, whose slope and relative height were already estimated, was convoluted by the fitted peak function to give the experimental low-energy tail. When other peaks from the target contaminants appeared near the main peak, their heights were estimated by fitting the spectrum assuming the same peak-tail shape for all the peaks as shown in Fig. 2. The peaks and tails from the contaminants and the tail of the main peak were then subtracted from the energy spectrum. Finally, the counts in the main peak were obtained by summing directly the counts in the resulting spectrum within the width at $1/20$ maximum and by adding the counts outside the width which were estimated from the fitted peak functions. The counts outside

the width were about 1% of the total counts.

The nuclear reactions in a detector decrease the peak counts and increase the tail counts. From the detection efficiencies for protons [22] and for deuterons [23], the reduction of the peak counts was estimated to be $0.6 \pm 0.1\%$ for 18 MeV protons and $0.55 \pm 0.1\%$ for 16 MeV deuterons, and $0.1 \pm 0.1\%$ for 9 MeV protons and 8 MeV deuterons. The peak counts obtained above were corrected for the reduction using the estimated detection efficiency.

The background caused by the contaminant peaks was less than 0.4% of the main peak counts at $\theta_{\text{lab}} \geq 20^\circ$ for the incident beam energies above 5 MeV. However, it increased up to 3.5% in the 16° spectrum at the lowest energy of 2 MeV where protons scattered in the target window foils were observed to contribute to the background. At the incident energies of 2–9 MeV where the counter telescopes were not used, the tail of the elastically scattered protons was estimated to make the background of up to 1.5% in the recoil deuteron counts. The uncertainty in the cross section due to the background subtraction was estimated to be 0.7% at the maximum.

The beam charge collected by the Faraday cup was measured by a current integrator (Ortec 439) which was calibrated to 0.2%. The measured charge was corrected for the low-energy component of the beam (hereafter temporarily called beam halo) which was mainly caused by the edge-scattering at the beam collimating slit. Since the observed particle spectrum includes the information on the energy distribution of the beam and especially the beam halo contributes to the tail part of the spectrum, the relative fraction of the halo was estimated from the integrated tail counts in the following way.

The small amount of the tail counts caused by the nuclear reactions in the detector was estimated as the peak reduction as described above, and was subtracted from the total tail counts. The edge scattering at the counter slits (both A and B systems) was found, from the separate measurements using counter slits of various apertures, to make a $25 \pm 10\%$ contribution to the remaining tail counts. The double scattering in the target cell windows and in the target gas also contributes to the tail and the amount was estimated to be less than 10%. The contribution of the beam halo was therefore estimated to have a $65 \pm 20\%$ fraction in the tail counts. These results were in accord with the estimations based on the formulas for the edge scattering [24]. From the ratio of the halo contribution in the tail to the peak counts, the low-energy component of the beam (beam halo) collected in the Faraday cup was estimated to be $1.0 \pm 0.5\%$ at 5 MeV and $1.2 \pm 0.6\%$ at 18 MeV. This estimation caused the largest error for the final cross section except for the background subtraction procedure at very forward angles.

The dead time in the counter was kept at a level below 0.4% by controlling the beam intensity. For the dead time estimation, pulser signals generated at a rate proportional to the beam intensity were counted in the counters together with the particle events.

The isotopic enrichment of the target gas was 99.75%. The target gas pressure was measured with a mercury

manometer to an accuracy of $\pm 0.2\%$ when the gas was charged into the target cell, and the relative variation was monitored during the experiment by measuring the elastic scattering as described in Sec. III A.

The solid angle times the effective target thickness for the counter was calculated at every angle. The correction due to the finite size of the beam was sufficiently small, and the uncertainties of $\pm 0.2\%$ of the calculated values mainly came from those in the slit geometry.

The cross sections measured by the left and right counters agreed within about $\pm 0.3\%$, and were averaged to give the final results. The total uncertainty in the final cross section was in the range from 0.6% to 1.1% and typically 0.8%.

In order to check the present experimental procedure, the differential cross section of the $p + p$ scattering was measured by the same method at several angles at the beam energies of 5, 9.85, and 12 MeV. The experimental results were 0.4%–0.9% higher than the results calculated from the Paris potential [25] at 5 MeV and 0.5–0.7% lower at 9.85 and 12 MeV. The differences were within the experimental errors.

IV. EXPERIMENTAL RESULTS

The present data on the $p + d$ cross section at $E_p = 2$ –18 MeV were compared with the previous data at 1–10 MeV [26], 8.5–22.7 MeV [9], 10–14.1 MeV [10], 10.04 MeV [27], 12.18 MeV [28], and at 13.93 MeV [29]. The whole data showed excellent agreements except at a few forward angles. Examples of the data at 5 and 10 MeV are shown in Fig. 3. The present data have as consistently small errors as 0.6%–1.1%.

The $\vec{p} + d A_y$ data at $E_p = 5$ –18 MeV were compared with the previous ones at 5–22.7 MeV [8,9], 10–14.1 MeV [10], 11.1 MeV [11], and at 14.1 MeV [12]. As partly shown for 5 and 10 MeV in Fig. 4, the A_y data also agreed within experimental errors. The A_y peak appears around 120° as seen in the figure. The experimental peak heights are compared in Fig. 5, where one may again see good agreements among the whole data, together with the high accuracy and the smooth energy dependence in the present data. It is to be mentioned that the accuracies of A_y (typically of 0.0009) in the present measurement are factors of 3–5 smaller than those of the previous reports.

The angular distributions of the cross section and analyzing power are presented in Figs. 6–9 at 1 MeV intervals for the incident energies of 5–9 MeV and at 2 MeV intervals for 10–18 MeV. Most of the experimental errors are within the sizes of the data points. The data may be seen to vary quite smoothly with angle and systematically with energy. As the incident energy increases, the cross section decreases monotonically and the minimum around 120° gradually moves backward (Figs. 6 and 7). The A_y peak becomes higher with the energy and moves backward as well, as seen in Figs. 8 and 9.

Since the A_y peak has a broad width, the peak height can be well determined experimentally from the angular distribution of A_y . The same is true for the cross-

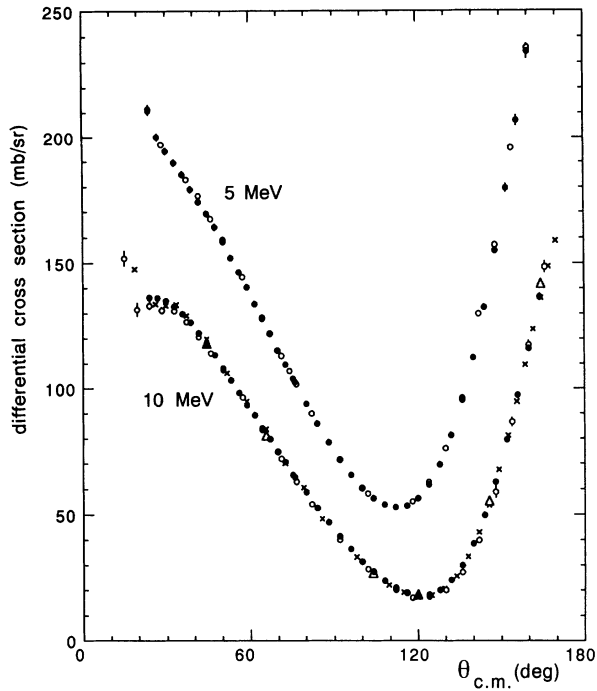


FIG. 3. Experimental data for the differential cross sections in the $p + d$ scattering at $E_p = 5$ and 10 MeV. The present data (closed circle) are compared with the data from Ref. [26] (open circle), Ref. [9] (cross), and Ref. [27] (triangle). Error bars within the sizes of the symbols are not shown.

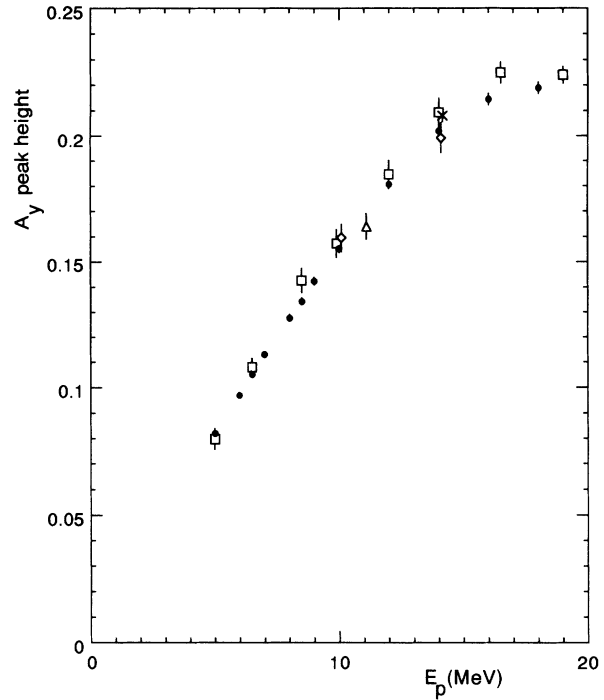


FIG. 5. Experimental data for the height of the $\bar{p} + d$ A_y peak around 120° . The present data (closed circle) are compared with the data from Refs. [8,9] (open square), Ref. [10] (diamond), Ref. [11] (triangle), and Ref. [12] (cross).

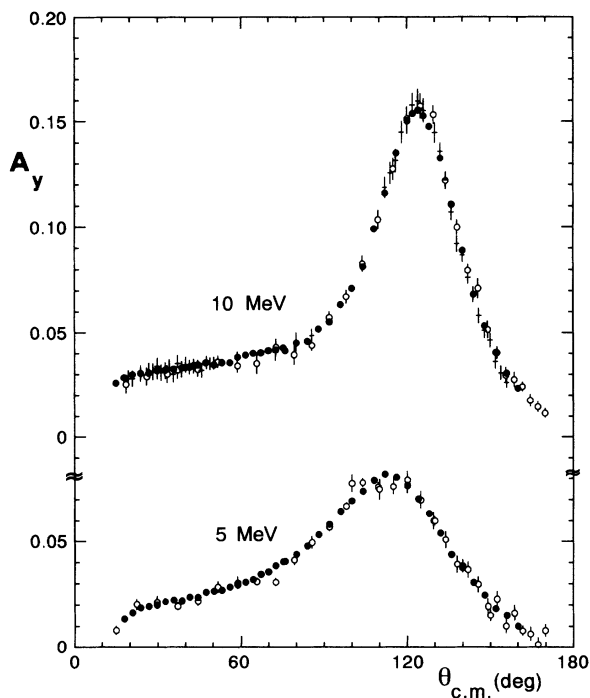


FIG. 4. Experimental data for the vector analyzing power A_y in the $\bar{p} + d$ scattering at $E_p = 5$ and 10 MeV. The present data (closed circle) are compared with the data from Refs. [8,9] (open circle) and Ref. [10] (cross). Error bars within the sizes of the symbols are not shown.

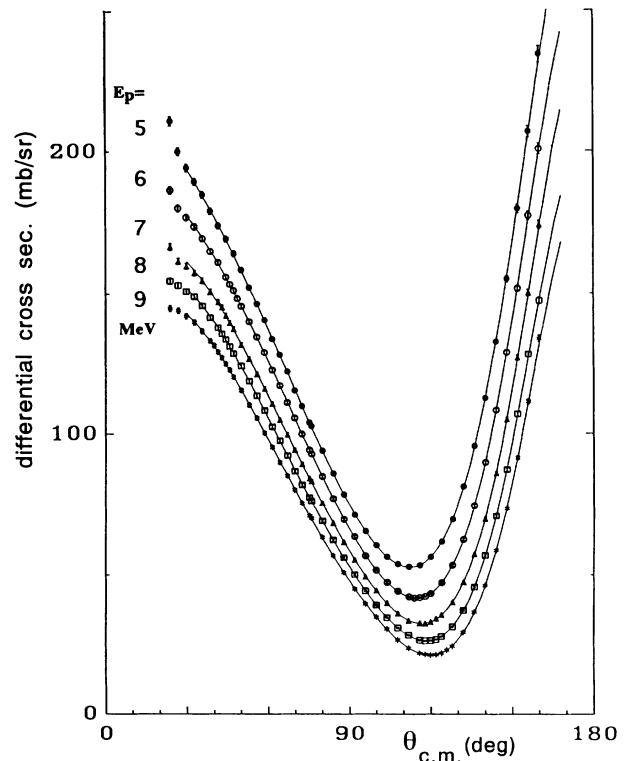


FIG. 6. Differential cross sections in the $p + d$ scattering at $E_p = 5, 6, 7, 8,$ and 9 MeV. Curves are the results of the Legendre fit to the data (see text) in the range of $\theta \geq 40^\circ$. Error bars within the sizes of the symbols are not shown.

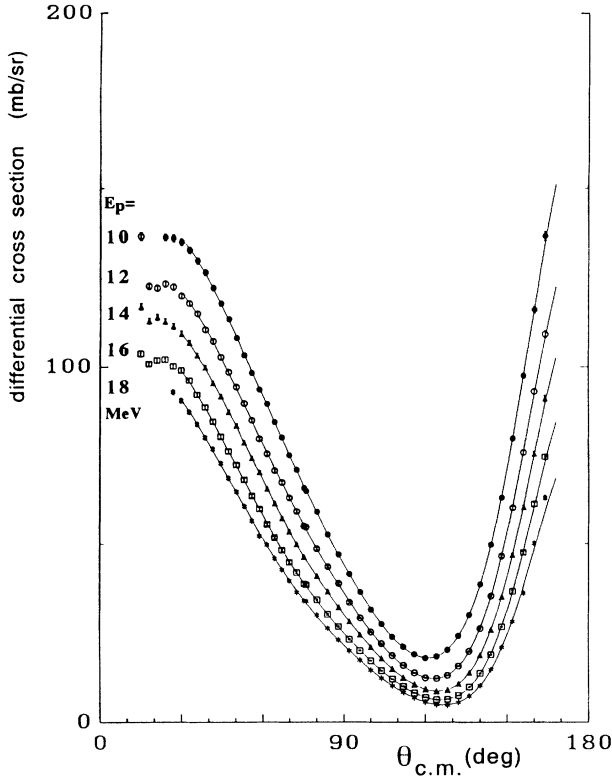


FIG. 7. The same as in Fig. 6 at $E_p = 10, 12, 14, 16,$ and 18 MeV.

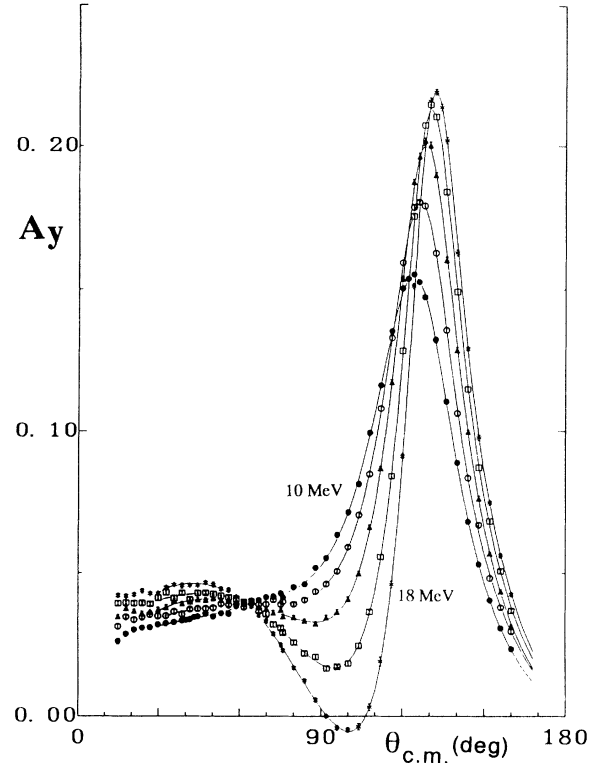


FIG. 9. The same as in Fig. 8 at $E_p = 10$ (closed circle), 12 (open circle), 14 (triangle), 16 (square), and 18 (cross) MeV.

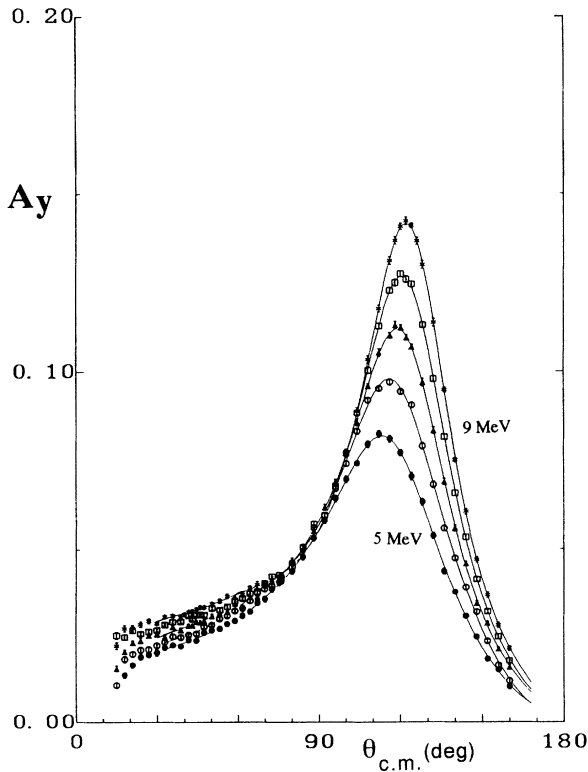


FIG. 8. Analyzing power A_y in the $\bar{p} + d$ scattering at $E_p = 5$ (closed circle), 6 (open circle), 7 (triangle), 8 (square), and 9 (cross) MeV. Curves are the results of the Legendre fit to the data in the range of $\theta \geq 40^\circ$. Error bars within the sizes of the symbols are not shown.

section minimum. Moreover, both the A_y peak height and the cross-section minimum change slowly with energy. Hence, it seems useful to derive them as the convenient quantities in the comparisons of the experiment with the calculation. For this purpose, the experimental cross section σ and A_y were fitted at each energy to the Legendre polynomials of

$$\sigma = \sum_{L=0}^{L_{\max}} a_L(E) P_L(\theta), \quad (6)$$

$$\sigma A_y = \sum_{L=0}^{L_{\max}} b_L(E) P_L^1(\theta). \quad (7)$$

Because the angular distribution of σ was complicated at forward angles due to the interference between the Coulomb and nuclear interactions, the fitting was made for the data in the range of $\theta_{c.m.} \geq 40^\circ$. By setting L_{\max} at 9, excellent fits were obtained for both σ and A_y in the whole energy range as shown in Figs. 6–9 by the solid curves. From the fitted curves, the cross-section minimum and the A_y peak height together with their positions (angles) were evaluated. The results are presented in Table I, where those for the A_y at 2–4 MeV from our separate measurements [30] are also included. The angle for the cross-section minimum and that for the A_y peak are not the same, and the difference increases with the incident energy. The values in the table are compared with the calculation in the next section.

TABLE I. The minimum of the differential cross section, the maximum of A_y , and their positions (angles), evaluated from the Legendre fit to the present data. The results from the separate measurement [30] are also listed.

| E_p (MeV) | Cross section minimum | | | | Analyzing power maximum | | | |
|-------------|-----------------------|----------------|-----------------------|----------------|-------------------------|--------------|-----------------------|----------------|
| | σ (mb/sr) | $\Delta\sigma$ | $\theta_{c.m.}$ (deg) | $\Delta\theta$ | A_y | ΔA_y | $\theta_{c.m.}$ (deg) | $\Delta\theta$ |
| 2.00 | 123.65 | 0.93 | 94.38 | 0.33 | 0.0329 | 0.0004 | 94.79 | 1.08 |
| 2.50 | 104.88 | 0.71 | 99.85 | 0.26 | 0.0420 | 0.0003 | 99.38 | 0.51 |
| 3.00 | 91.10 | 0.56 | 103.44 | 0.20 | 0.0493 | 0.0006 | 103.52 | 0.57 |
| 4.00 | 69.77 | 0.39 | 108.72 | 0.17 | 0.0661 | 0.0006 | 109.52 | 0.34 |
| 5.00 | 52.71 | 0.29 | 112.30 | 0.15 | 0.0814 | 0.0007 | 113.12 | 0.31 |
| 6.00 | 41.82 | 0.22 | 114.71 | 0.14 | 0.0976 | 0.0007 | 115.80 | 0.22 |
| 6.50 | 37.17 | 0.20 | 116.01 | 0.13 | 0.1047 | 0.0007 | 117.36 | 0.22 |
| 7.00 | 32.85 | 0.18 | 116.75 | 0.14 | 0.1120 | 0.0006 | 118.79 | 0.19 |
| 8.00 | 26.71 | 0.14 | 118.56 | 0.13 | 0.1270 | 0.0006 | 120.47 | 0.15 |
| 8.50 | 24.34 | 0.13 | 119.39 | 0.13 | 0.1346 | 0.0006 | 121.37 | 0.13 |
| 9.00 | 21.76 | 0.12 | 119.98 | 0.13 | 0.1419 | 0.0007 | 112.07 | 0.14 |
| 10.00 | 18.01 | 0.10 | 120.97 | 0.13 | 0.1549 | 0.0007 | 123.89 | 0.12 |
| 12.00 | 12.19 | 0.07 | 123.11 | 0.12 | 0.1811 | 0.0009 | 126.39 | 0.11 |
| 14.00 | 8.66 | 0.05 | 124.48 | 0.12 | 0.2019 | 0.0009 | 128.46 | 0.11 |
| 16.00 | 6.22 | 0.04 | 125.72 | 0.12 | 0.2142 | 0.0012 | 130.40 | 0.11 |
| 18.00 | 4.73 | 0.03 | 126.65 | 0.11 | 0.2206 | 0.0016 | 131.97 | 0.10 |

V. COMPARISON WITH FADDEEV CALCULATION

For comparison with the experiment, a Faddeev calculation based on the realistic Paris NN potential was carried out using a computer code by Takemiya [16]. The total angular momenta of up to 2 were included in the NN subsystem, and those of up to 19/2 in the $3N$ system. Coulomb force in the $p + d$ system was treated approximately in the code in the same manner as introduced by Doleschall [31].

The calculated results reproduce well the gross structure of the differential cross section, as seen in Figs. 10 and 11. The Coulomb-nuclear interference effect in the cross section at forward angles is fairly well reproduced with the approximate treatment of Coulomb force. However, the following disagreements are recognized. At incident energies below 5 MeV, the calculated cross section is a little larger than the experimental one in the whole angular range. As the energy increases, the calculation decreases somewhat more rapidly than the experiment, and above 12 MeV it comes below the experiment in the whole angular range. The approximation in the Coulomb force treatment may be responsible for the disagreement. A nearly correct treatment of Coulomb force has been performed at 2.5 MeV by Berthold, Stadler, and Zankel [15]. The cross section predicted by the calculation is about 20% smaller at forward angles than that calculated in the approximate treatment of Coulomb force. At backward angles, both the treatments give nearly the same cross section. Hence, the disagreement at forward angles seen in Figs. 10 and 11 would have come mainly from the inadequacy of the Coulomb force treatment, while the disagreement at backward angles is considered to indicate the presence of some shortcoming in the nuclear potential used in the calculation.

The calculated and experimental results for the $\vec{p} + d$

A_y are shown in Figs. 12 and 13, where the existing data for the $\vec{n} + d$ A_y [4-7] are also included. Three kinds of discrepancies between the calculation and the experiment are observed. First, at forward angles of $\theta_{lab} \leq 40^\circ$, the calculation is slightly below the experiment in the whole energy range from 5 to 18 MeV. Second, as is well known,

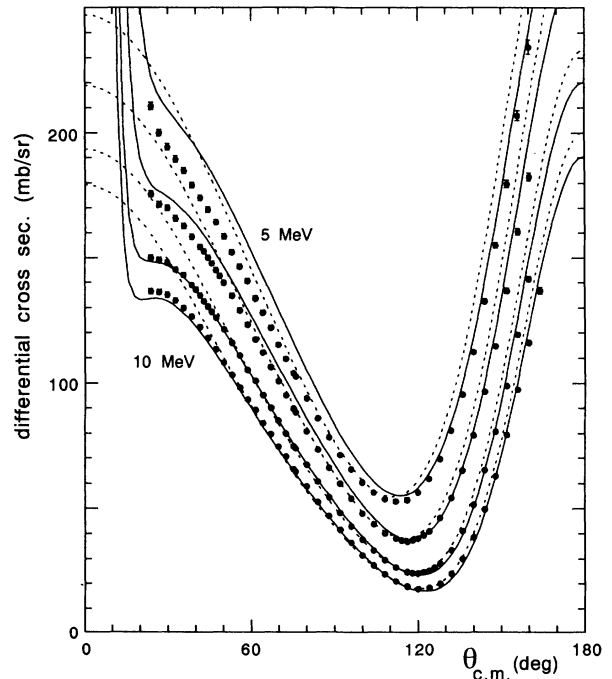


FIG. 10. Differential cross section in the $p + d$ scattering at $E_p = 5$ (top), 6.5, 8.5, and 10 MeV (bottom). The solid (dashed) curves are the results of the Faddeev calculation Ref. [16] for the $p + d$ ($n + d$) scattering using the Paris NN potential.

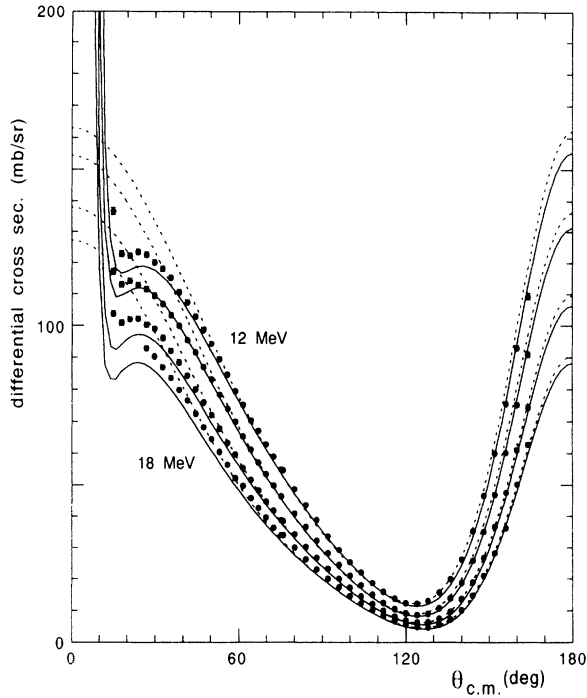


FIG. 11. The same as in Fig. 10 at $E_p = 12$ (top), 14, 16, and 18 MeV (bottom).

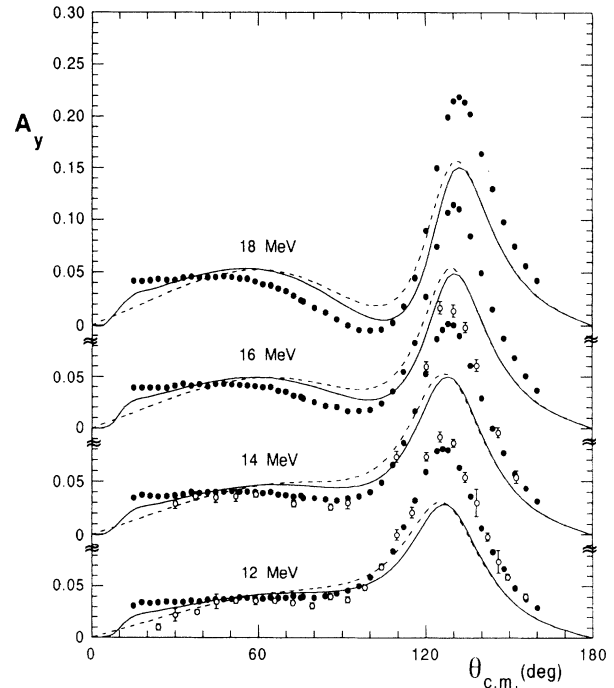


FIG. 13. The same as in Fig. 12 at 12, 14, 16, and 18 MeV. The $\bar{n} + d$ data are from Refs. [5,6].

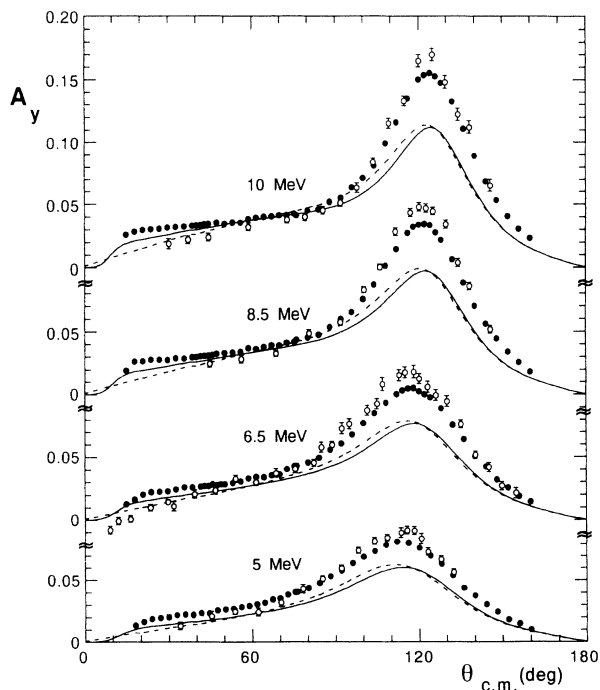


FIG. 12. Analyzing power A_y in the $\bar{p} + d$ (closed circle) and the $\bar{n} + d$ (open circle) scatterings at 5, 6.5, 8.5, and 10 MeV. The solid (dashed) curves are the results of the Faddeev calculation [16] for $p + d$ ($n + d$) scattering using the Paris NN potential. The $\bar{n} + d$ data are from Refs. [4,7].

the calculated values for the heights of the $\bar{p} + d$ and $\bar{n} + d$ A_y peaks are about 25% smaller than the experimental ones at all the energies. Third, the experimental difference in the A_y peak heights between the $\bar{p} + d$ and the $\bar{n} + d$ scatterings is much larger than the calculated difference.

The first discrepancy may be attributed largely to the approximate treatment of Coulomb force as discussed above. The third one might suggest the charge symmetry breaking in the nuclear interactions and is discussed in more detail later.

The second discrepancy for the A_y peak height has been pointed out [32,33] to originate from the inadequate 3P_J state NN interactions used in the calculation. As described earlier, Witala and Glöckle [13] have shown that the discrepancy can be removed if one assumes strong charge independence breaking in the strengths of the 3P_J state NN interactions. The breaking they supposed is of the order of 10%. An attempt to reproduce the experimental data without symmetry breaking has been done by Takemiya [14] who introduced an increased strength for the short range (~ 1.5 fm) part of the LS force in the Paris NN potential. The results of his calculation for A_y are shown in Fig. 14, where the modification of the potential is the same for all the incident energies. The large discrepancy around the A_y peak almost disappears at 5 and 10 MeV, though an appreciable discrepancy still remains at 18 MeV. At low energies as in the present case, the effect of the short-range force is expected to arise mainly from the off-energy-shell interaction. The above results may therefore indicate that the A_y peak height

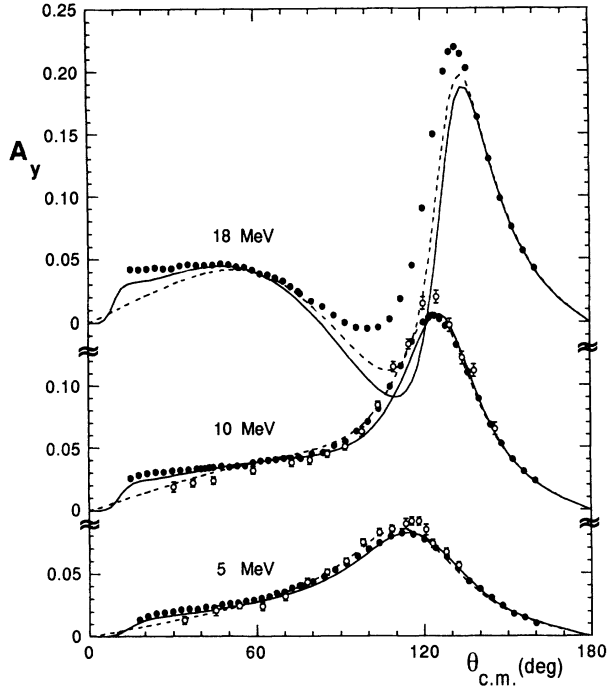


FIG. 14. Analyzing power A_y in the $\bar{p} + d$ (closed circle) and the $\bar{n} + d$ (open circle) scattering at 5, 10, and 18 MeV. The solid (dashed) curves are the results of the Faddeev calculation [16] for the $p + d$ ($n + d$) scattering using the Paris NN potential whose LS force is modified (see text).

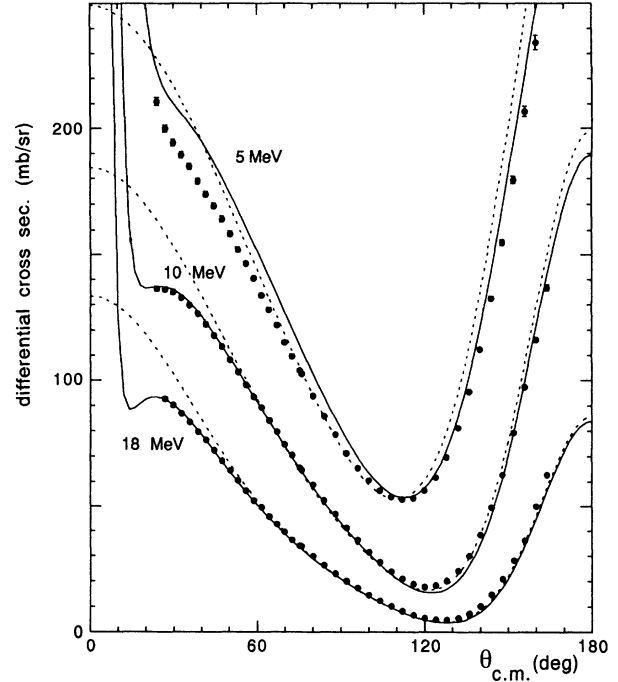


FIG. 15. Differential cross section in the $p + d$ scattering at 5, 10, and 18 MeV. The curves show the same calculation as in Fig. 14.

is affected by the off-energy-shell LS interaction. Figure 15 shows the results of the same calculation for the cross section. When compared with Figs. 10 and 11, the modification in the LS force is seen to cause only a little change in the cross section.

The experimental values of the A_y peak height and the cross-section minimum have been determined earlier from the Legendre fit to the present data. A quantitative comparison of the experiment with the calculation may be most conveniently made using these values.

We define a fractional discrepancy between the calculation and the experiment in the A_y peak height as $\Delta A_y = (A_y^{\text{calc}} - A_y^{\text{exp}})/A_y^{\text{exp}}$ using the calculated and experimental values of A_y^{calc} and A_y^{exp} . The energy dependence of ΔA_y is shown in Fig. 16, where our experimental results at 2–4 MeV from the separate measurement [30] are also included. The discrepancy takes large negative values ranging from -13% at 2 MeV to -40% at 18 MeV for the calculation based on the original Paris NN potential. When the short range part of the LS potential is modified, the calculated A_y peak height is pushed up by about 23% nearly independently of the beam energy and the discrepancy becomes moderate as shown by the open circles in Fig. 16.

However, the energy dependence of the discrepancy ranging from $+10\%$ at 2 MeV to -15% at 18 MeV is still not accounted for by the modification. The approximate treatment of Coulomb force in the $p + d$ calculation, from which the above results were evaluated, might be respon-

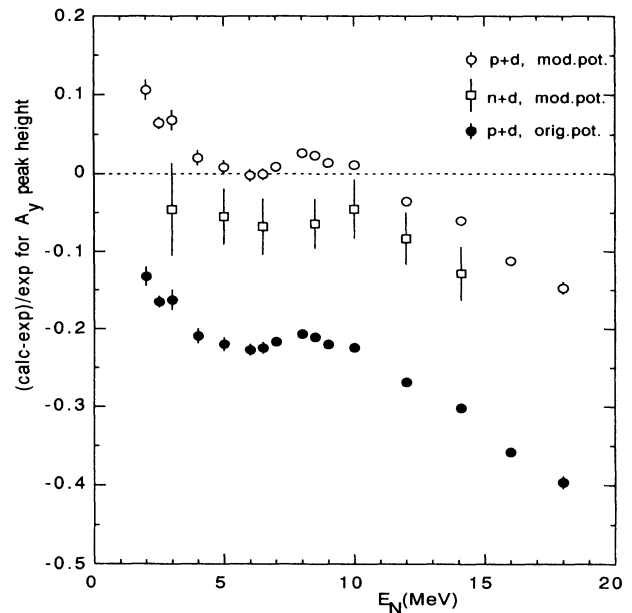


FIG. 16. Fractional discrepancy of the A_y peak height, $\Delta A_y = (A_y^{\text{calc}} - A_y^{\text{exp}})/A_y^{\text{exp}}$, between the present $p + d$ data and Faddeev calculation [16] using the original Paris NN potential (solid circle). The open circle (open square) shows the discrepancy between the $p + d$ data ($n + d$ data from Refs. [3–7]) and the calculations using the modified LS force in the NN potential.

sible for the discrepancy. At 2.5 MeV, Coulomb force in the $p+d$ scattering has been treated nearly correctly [15]. The “correct” height of the $\bar{p}+d A_y$ peak is about 12% lower than that calculated in the approximate treatment of Coulomb force. Hence, ΔA_y in a correct Coulomb calculation using the modified potential at 2.5 MeV would become -6% which is 12% below the value predicted in the approximate Coulomb calculation. The “correct” ΔA_y at 18 MeV is expected to be even smaller than the “approximate” value of -15% (see Fig. 16), because the correct treatment tends to lower the A_y peak height in the present energy region as discussed in the next section. Hence, it is certain that there remains an energy-dependent discrepancy which cannot be attributed to the inadequacy of the treatment of Coulomb force. Existence of the energy-dependent discrepancy for the $\bar{n}+d$ scattering can also be seen in Fig. 16, though the situation is not so clear due to the long error bars of the $\bar{n}+d$ data [3–7]. To eliminate the energy-dependent discrepancy in the A_y peak, some other improvements on the NN potential would be necessary.

The fractional discrepancy for the cross-section minimum, $\Delta\sigma = (\sigma^{\text{calc}} - \sigma^{\text{exp}})/\sigma^{\text{exp}}$, was also evaluated in the same manner as shown in Fig. 17. It is to be noted that $\Delta\sigma$ takes even large values at both the ends of the energy range of the measurement, and is strongly energy dependent. The width of the variation in the range 2–18 MeV is 43% which is larger than the width for ΔA_y (27%) calculated from the original NN potential. The approximate Coulomb calculation is not considered the main cause for this discrepancy, because the cross-section minimum predicted in the “correct” Coulomb calculation [15] deviates from the approximate Coulomb calculation only by about 5% at 2.5 MeV and the difference is expected to be within several % in the whole energy range 2–18 MeV. The modification in the short range part of the LS potential, which has been effective for ΔA_y , seems

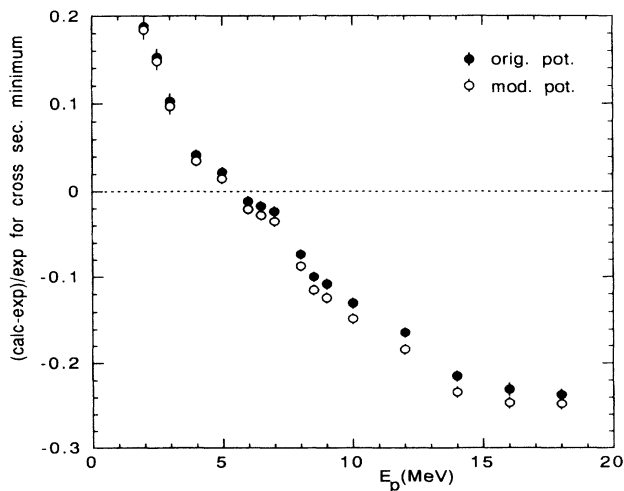


FIG. 17. Fractional discrepancy of the cross-section minimum, $\Delta\sigma = (\sigma^{\text{calc}} - \sigma^{\text{exp}})/\sigma^{\text{exp}}$. The present $p+d$ data are compared with the Faddeev calculations [16] using either the original Paris NN potential (solid circle) or the Paris NN potential whose LS force is modified (open circle).

to have essentially no effect on $\Delta\sigma$ as shown in Fig. 17. The large discrepancy in the cross section might indicate that some improvement is necessary also in the scalar part of the NN potential.

VI. COMPARISON WITH $\bar{n}+d$ DATA

The difference between the $n+d$ and the $p+d$ systems is in the presence of different pairs of interacting particles of nn and pp . If the difference in the physical observables between the $n+d$ and the $p+d$ systems cannot be fully attributed to the presence of Coulomb force in the $p+d$ system, it necessarily indicates the charge symmetry breaking (CSB) in the nuclear force. The comparison between the heights of the $\bar{n}+d$ and the $\bar{p}+d A_y$ peaks is of special interest in studying the difference between the $n+d$ and the $p+d$ systems, because (a) the two A_y peaks appear at almost the same scattering angles, (b) the difference between the peak heights is large, and (c) the peak heights can be measured accurately.

The $\bar{p}+d A_y$ peak heights have already been evaluated from the Legendre fit to the present experimental data in Sec. IV. The $\bar{n}+d$ peak heights were evaluated from the $\bar{n}+d A_y$ data in Refs. [3–7] in the same manner as used for deriving the $\bar{p}+d A_y$ peak heights. In this fit, the present $p+d$ cross section data were used for σ in Eq. (7), because the $n+d$ cross-section data are lacking and have large experiment errors. An excellent fit was obtained for the $\bar{n}+d A_y$. The differences between the $\bar{n}+d$ and the $\bar{p}+d A_y$ peak heights evaluated for the same beam energies are shown in Fig. 18. Since the present experiment provides enough accurate data on the $\bar{p}+d A_y$, the errors in the differences come mainly from the scale uncertainties (3–6%) of the $\bar{n}+d A_y$ data. Figure 18(a) shows that the absolute value of the difference has a tendency to increase with the energy, while Fig. 18(b) shows that the relative value seems to be nearly constant above 5 MeV.

The difference predicted by the Faddeev calculation with the approximate Coulomb treatment for the $p+d$ system in Ref. [31], is also shown by dashed curves in Fig. 18. Although the relative energy dependence seems to be qualitatively reproduced by the calculation, the absolute value is much smaller than the experiment in the whole energy range 3–14.1 MeV. The difference at 2.5 MeV predicted by the Faddeev calculation with the nearly exact Coulomb force [15] is also shown by the open circles in Fig. 18. The predicted value is much larger than the approximate Coulomb calculation, and seems to be close to the experimental value. However, the large experimental uncertainty at 3 MeV obscures the conclusion to be drawn on CSB.

When the NN potential used in the calculation is changed from the original Paris potential to the LS -modified potential, the A_y peak height is increased by about 23% as described in the previous section. However, the difference between the $\bar{n}+d$ and the $\bar{p}+d A_y$ peak heights was found to remain essentially the same. This might indicate that CSB can be most effectively studied from the peak height difference.

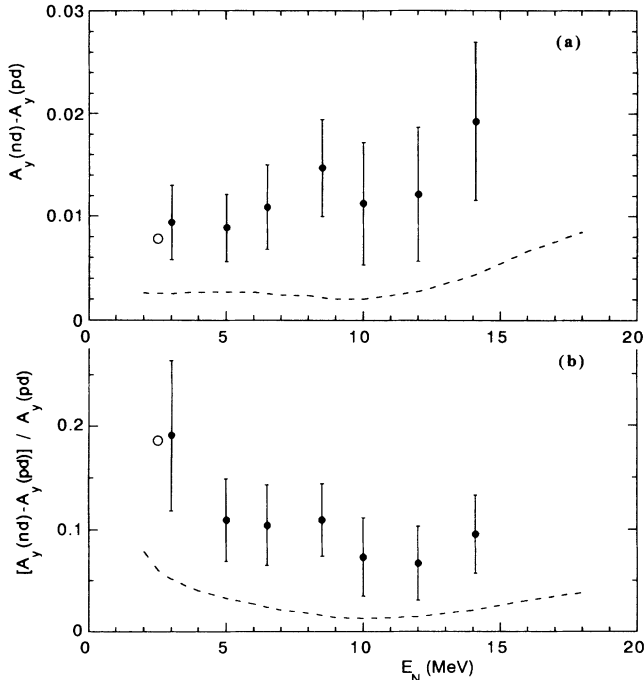


FIG. 18. Difference in the peak height between the $\bar{n} + d A_y$ and $\bar{p} + d A_y$. In the lower figure, the difference is normalized by the $\bar{p} + d A_y$ peak height. The closed circles indicate the experimental values obtained from the present $p + d$ data and the $n + d$ data from Refs. [3–7]. For the comparison with the $\bar{n} + d A_y$ data at 14.1 MeV, an interpolated value of the $\bar{p} + d A_y$ was used. The dashed curve denotes the calculation in which the Coulomb force is treated approximately as in Ref. [31]. The open circles show the result of the nearly correct treatment of Coulomb force [15].

For further investigation, accurate experiments on the A_y peak height difference below the deuteron breakup threshold are of great use, because the nearly correct treatment of Coulomb force has already been developed in this energy range. However, if similar calculations were available above the threshold, CSB can be investigated more clearly at higher energies where the effect is considered relatively conspicuous. It is evident that the experimental accuracy of Fig. 18 is not satisfactory. Since the precise data have been provided for the $\bar{p} + d A_y$ in the present experiment, equally precise data on the $\bar{n} + d A_y$ in the same energy range are of great interest. At the same time, correct Coulomb calculations above the threshold are highly desired.

VII. SUMMARY

Precise and systematic measurements on the differential cross section and vector analyzing power A_y of the $p + d$ scattering were made at $E_p = 5, 6, 6.5, 7, 8, 8.5, 9, 10, 12, 14, 16,$ and 18 MeV. The differential cross section was measured also at $E_p = 2, 2.5, 3,$ and 4 MeV. The statistical error for A_y was typically 0.0009 and the scale uncertainty was within 0.7%. The total error for the cross section was typically 0.8%. The experimental

accuracy was much improved especially for A_y . The data show sufficiently smooth dependence on both angle and energy, and on the whole agree with the previous data.

The data were compared with the Faddeev calculation using the Paris NN potential together with the conventional approximation for Coulomb force. The angular distributions of A_y and the cross section were fairly well reproduced. However, the calculation underestimates the A_y peak height by 23% at $E_p = 5$ MeV and by 40% at 18 MeV, and the prediction for the cross-section minimum is 19% above the experiment at 2 MeV and 24% too small at 18 MeV. These large and energy-dependent discrepancies seem not to be fully attributed to the approximate nature of the Coulomb force treatment.

The discrepancy in A_y is largely reduced if the short range part of the LS force in the Paris NN potential is modified [14]. This means that the off-energy-shell LS interaction plays an important role for A_y . However, the energy dependence of the discrepancy in A_y was found to still remain unchanged, which suggests that some other improvement on the NN potentials is necessary. Although a definite conclusion cannot be made at this moment, an introduction of strong charge independence breaking and charge symmetry breaking (CSB) in 3P_J state NN interactions [13] might be one of the directions of the improvement. The large discrepancy at the cross-section minimum was noticed in the present work. The modification of the LS potential has no appreciable effect on this discrepancy. An improvement of the scalar part of the NN interaction would be necessary to reduce the discrepancy.

The present $\bar{p} + d A_y$ data were compared with the $\bar{n} + d A_y$ data at 3–14.1 MeV [3–7]. The difference in the A_y peak height between the $\bar{p} + d$ and the $\bar{n} + d$ scatterings was several times larger than the prediction of the Faddeev calculation with the approximate treatment of the Coulomb force. To extract a definite conclusion on CSB, precise $\bar{n} + d A_y$ data of about 1% accuracy are necessary together with the correct Coulomb calculations above the deuteron breakup threshold.

One of the aims of the study on the $3N$ systems is to extract information on the nuclear interactions which are hardly or never obtained from the $2N$ observables. The precise and systematic data presented in this report on the $\bar{p} + d A_y$ and the cross section would serve as experimental data standards in this kind of study. Our further measurements of the vector and tensor analyzing powers of the $p + d$ scattering below the deuteron breakup threshold will be reported elsewhere [30].

ACKNOWLEDGMENTS

The authors wish to thank Professor T. Takemiya for his intimate communications and his permission of the use of his computer code, Professor Y. Koike, Professor S. Oryu, and Professor W. Gruebler for their valuable discussions, Y. Koga and T. Maeda for preparing experimental instruments, and N. Nishimori, S. Ueno, and T. Miwa for their help during the cross-section measurement.

- [1] T. Takemiya, *Prog. Theor. Phys.* **74**, 301 (1985).
- [2] H. Witala, W. Glöckle, and T. Cornelius, *Few-Body Syst.* **3**, 123 (1988); H. Witala, W. Glöckle, and T. Cornelius, *Nucl. Phys.* **A491**, 157 (1989).
- [3] J. E. McAninch, W. Haeberli, H. Witala, W. Glöckle, and J. Golak, *Phys. Lett. B* **307**, 13 (1993).
- [4] W. Tornow, C. R. Howell, M. Alohal, Z. P. Chen, P. D. Felsher, J. M. Hanly, R. L. Walter, G. Weisel, G. Mertens, I. Slaus, H. Witala, and W. Glöckle, *Phys. Lett. B* **257**, 273 (1991).
- [5] C. R. Howell, W. Tornow, K. Murphy, H. G. Pfützner, M. L. Roberts, Anli Li, P. D. Felsher, R. L. Walter, I. Slaus, P. A. Treado, and Y. Koike, *Few Body Syst.* **2**, 19 (1987).
- [6] W. Tornow, R. C. Byrd, C. R. Howell, R. S. Pedroni, and R. L. Walter, *Phys. Rev. C* **27**, 2439 (1983).
- [7] W. Tornow, C. R. Howell, R. C. Byrd, R. S. Pedroni, and R. L. Walter, *Phys. Rev. Lett.* **49**, 312 (1982).
- [8] R. E. White, W. Grüebler, B. Jenny, V. König, P. A. Schmelzbach, and H. R. Bürgi, *Nucl. Phys.* **A321**, 1 (1979).
- [9] W. Grüebler, V. König, P. A. Schmelzbach, F. Sperisen, B. Jenny, R. E. White, F. Seiler, and H. W. Roser, *Nucl. Phys.* **A398**, 445 (1983).
- [10] G. Rauprich, H. J. Hähn, M. Kuras, P. Niessen, K. R. Nyga, H. Oswald, L. Sydow, H. Paetz gen Schieck, and Y. Koike, *Few-Body Syst.* **5**, 67 (1988).
- [11] M. Sawada, S. Seki, K. Furuno, Y. Tagishi, Y. Nagashima, J. Shimizu, M. Ishikawa, T. Sugiyama, L. S. Chuang, W. Grüebler, J. Sanada, Y. Koike, and Y. Taniguchi, *Phys. Rev. C* **27**, 1932 (1983).
- [12] J. C. Duder, M. Sosnowski, and D. Melnik, *Phys. Lett. B* **85**, 206 (1979).
- [13] H. Witala and W. Glöckle, *Nucl. Phys.* **A528**, 48 (1991).
- [14] T. Takemiya, *Prog. Theor. Phys.* **86**, 975 (1991).
- [15] G. H. Berthold, A. Stadler, and H. Zankel, *Phys. Rev. C* **41**, 1365 (1990).
- [16] T. Takemiya, private communication.
- [17] K. Sagara, K. Maeda, H. Nakamura, M. Izumi, T. Yamaoka, Y. Nishida, M. Nakashima, and T. Nakashima, *Nucl. Instrum. Methods A* **270**, 444 (1988).
- [18] R. A. Arndt, L. D. Roper, and R. L. Shotwell, *Phys. Rev. C* **3**, 2100 (1971).
- [19] P. Schwandt, T. B. Clegg, and W. Haeberli, *Nucl. Phys.* **A163**, 432 (1971).
- [20] D. C. Dodder, G. M. Hale, N. Jarmie, J. H. Jett, P. W. Keaton, Jr., R. A. Nisley, and K. Witte, *Phys. Rev. C* **15**, 518 (1977).
- [21] J. B. Marrion and B. A. Zimmermen, *Nucl. Instrum. Methods* **51**, 93 (1967).
- [22] M. Makino, R. Eisberg, K. Richie, R. Carlson, and C. Waddell, *Nucl. Instrum. Methods* **80**, 299 (1970).
- [23] T. R. King, J. J. Kraushaar, R. A. Ristinen, R. Smythe, and D. M. Stupin, *Nucl. Instrum. Methods* **88**, 17 (1970).
- [24] E. D. Courant, *Rev. Sci. Instrum.* **22**, 1003 (1951).
- [25] M. Lacombe, B. Louiseau, J. M. Richard, R. Vinh Mau, J. Côté, P. Pirès, and R. de Tournel, *Phys. Rev. C* **21**, 861 (1980).
- [26] D. C. Kocher and T. B. Clegg, *Nucl. Phys.* **A132**, 455 (1969).
- [27] N. Jaemie, R. E. Brown, and R. A. Hardekopf, *Phys. Rev. C* **29**, 2031 (1984).
- [28] W. T. H. van Oers and K. W. Brockman, Jr., *Nucl. Phys.* **21**, 189 (1960).
- [29] S. Kikuchi, J. Sanada, S. Suwa, I. Hayashi, K. Nishimura, and K. Fukunaga, *J. Phys. Soc. Jpn.* **15**, 9 (1960).
- [30] S. Shimizu, K. Sagara, H. Nakamura, K. Maeda, T. Miwa, N. Nishimori, S. Ueno, T. Nakashima, and S. Morinobu, to be submitted to *Phys. Rev. C*.
- [31] P. Doleschall, W. Grüebler, V. König, P. A. Schmelzbach, F. Sperisen, and B. Jenny, *Nucl. Phys.* **A380**, 72 (1982).
- [32] Y. Koike and J. Haidenbauer, *Nucl. Phys.* **A463**, 365c (1987).
- [33] H. Witala, W. Glöckle, and T. Cornelius, *Nucl. Phys.* **A496**, 446 (1989).

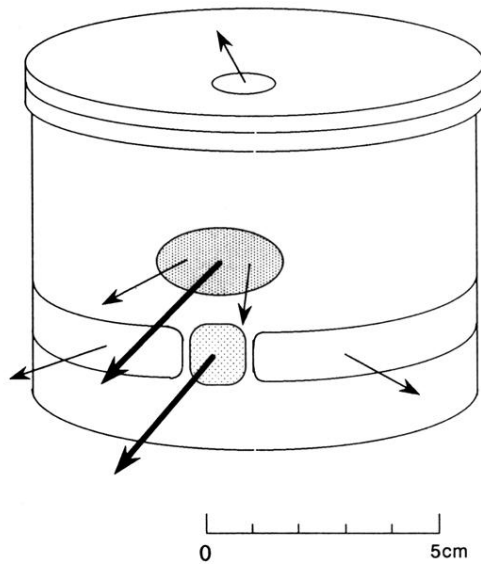


FIG. 1. Perspective view of the target gas cell. The thick and thin arrows indicate the incident beams and scattered particles, respectively. The upper and lower windows on the side were used for the measurements at forward angles ($\theta_{\text{lab}} \leq 16^\circ$) and backward angles, respectively. Through the window at the top, the elastic scattering was measured to monitor the target gas pressure. For the details of the window foils, see text. The shaded areas show the metal foils.